Interlayer bias effect on time-reversal symmetry breaking in twisted bilayer cuprates

Mathieu Bélanger and David Sénéchal

Département de Physique and Institut Quantique, Université de Sherbrooke, Sherbrooke, Québec, Canada J1K 2R1

We study a one-band Hubbard model of twisted bilayer cuprates with a twist angle of $53.13°$. By introducing an interlayer bias, we simulate heterobilayers of different dopings. Using the variational cluster approximation, we probe the effect of this bias on the time-reversal symmetry-breaking (TRSB) phase. Doping differences between layers affect the region where TRSB occurs; we construct a phase diagram mapping out the TRSB phase in the n_1-n_2 plane, with n_ℓ being the electron density on layer ℓ. We also map the spontaneous supercurrent on the same plane.

I. INTRODUCTION

Previous studies of the Hubbard model for twisted cuprates using the variational cluster approximation (VCA) at $\theta = 53.13°$ [1] and $43.60°$ [2] have shown that time-reversal symmetry is spontaneously broken in a narrow region of the superconducting dome when strong interlayer tunneling is considered. This shows that the time-reversal symmetry-breaking (TRSB) phase predicted around $45°$ [3–6] is strongly doping dependent. It was proposed that such a phase may lead to Majorana modes when in proximity with a material with spin-orbit coupling [7–9]. Superconducting qubits using twisted cuprates have been proposed [10]. Extensions to multilayer systems have also been studied [11].

The realization of two-dimensional monolayers of $Bi_2Sr_2CaCu_2O_{8+\delta}$ (Bi2212) with a transition temperature close to that of bulk samples [12,13] allows cuprate bilayers to be assembled in the laboratory and c-axis Josephson junctions to be created. Because of the d-wave pairing symmetry in each layer, the critical current changes depending on the twist angle in those junctions [14–17]. The critical current can remain finite at $45°$, pointing to the predicted TRSB phase [18,19].

Those junctions are challenging to make due to disorder inherent to Bi2212. It can thus be difficult for the two monolayers to be locally at the same doping. Indeed, the distribution of dopants can be inhomogeneous or the preparation process can introduce defects. On the other hand, it was proposed that some inhomogeneity could be needed in order to induce TRSB in twisted cuprate junctions [20].

Since changing the doping results effectively in a different material, one can take inspiration from the heterobilayer transition-metal dichalcogenides [21,22] and use different monolayer cuprates to create the bilayer system. The physics of cuprates being doping dependent, this would affect the TRSB phase.

The Hubbard model used in Refs. [1,2] can be modified to introduce a doping difference between the layers. This can also simulate the effect of defects or contamination in the junction-making process, leading to close, but different, doping content in each layer.

In this paper, we introduce an interlayer bias in the twisted cuprates Hubbard model at $\theta = 53.13°$ studied in Ref. [1]. This bias induces a doping difference between the two layers, allowing us to simulate heterobilayer cuprates. We show that the doping range where TRSB occurs is affected by interlayer bias. We obtain a phase diagram mapping out the TRSB phase in the n_1-n_2 plane, with n_ℓ being the electron density on layer ℓ. We also compute the spontaneous supercurrent circulating in a certain loop within the TRSB phase; this can be used as a TRSB order parameter.

II. MODEL

We use the Hamiltonian proposed in Ref. [1], where each layer is described by a one-band Hubbard model, and each site corresponding to a copper atom. To this layer Hamiltonian we add an interlayer bias term H_ϵ, so that the complete Hamiltonian is

$$H = H^{(1)} + H^{(2)} + H_\perp + H_\epsilon, \tag{1}$$

where the intralayer Hamiltonian $H^{(\ell)}$ is

$$H^{(\ell)} = \sum_{\mathbf{r},\mathbf{r}'\in\ell,\sigma} t_{\mathbf{r}\mathbf{r}'} c^\dagger_{\mathbf{r},\ell,\sigma} c_{\mathbf{r}',\ell,\sigma} + U \sum_{\mathbf{r}} n_{\mathbf{r},\ell,\uparrow} n_{\mathbf{r},\ell,\downarrow}$$
$$- \mu \sum_{\mathbf{r},\sigma} n_{\mathbf{r},\ell,\sigma}. \tag{2}$$

Here, $c_{\mathbf{r},\ell,\sigma}$ ($c^\dagger_{\mathbf{r},\ell,\sigma}$) is the annihilation (creation) operator of an electron at site $\mathbf{r}$ on layer ℓ with spin $\sigma =\uparrow, \downarrow$, and $n_{\mathbf{r},\ell,\sigma}$ is the number operator. $\mathbf{r}, \mathbf{r}'$ are the site indices of a square lattice for each layer. The on-site repulsion between electrons is U. The hopping matrix $t_{\mathbf{r}\mathbf{r}'}$ includes nearest-neighbor hopping (t) and next-nearest-neighbor hopping (t'). To describe Bi2212, we use the values $t = 1$, $t' = -0.3$, and $U = 8$, with t being the energy unit [1,2,23]. Nonlocal interactions were not considered since superconductivity can be driven by local repulsion alone and is resilient to nearest-neighbor repulsion at intermediate to strong coupling [24].

The coupling between the layers is provided by interlayer tunneling,

$$H_\perp = \sum_{n=1}^{3} V_n \sum_{\langle \mathbf{r}, \mathbf{r}' \rangle_{\perp,n,\sigma}} [c_{\mathbf{r},1,\sigma}^\dagger c_{\mathbf{r}',2,\sigma} + \text{H.c.}], \qquad (3)$$

with $\langle \mathbf{r}, \mathbf{r}' \rangle_{\perp,n,\sigma}$ representing the set of sites $\mathbf{r}$ on layer 1 and $\mathbf{r}'$ on layer 2, such that their projections on the plane are nth neighbors. We consider interlayer hopping up to third interlayer neighbors. The strength of the tunneling is given as in Ref. [2] by

$$V_n = V e^{-\lambda(|\mathbf{d_n}| - d_z)/a}, \qquad (4)$$

where $|\mathbf{d_n}| = |\mathbf{r} - \mathbf{r}'|$ is the three-dimensional distance between the two sites corresponding to the nth neighbors on different layers, d_z is the distance between the two layers, and a is the lattice constant of the square lattice. The interlayer tunneling between sites that are on top of each other is V. We use a damping parameter λ, the same as in Ref. [2]: $d_z = a$ and $\lambda = 11.13$. This set of parameters leads to similar interlayer tunneling as in Ref. [1]. We use $V = 0.4$ since a strong interlayer tunneling is needed to have a clear TRSB [1,2].

This model is obviously a simplification of actual cuprate bilayers. It neglects, among other things, the fact that each monolayer of Bi2212 contains two CuO_2 planes. It is based on a one-band effective model of each CuO_2 plane and ignores the precise structure of the interplane regions. Moreover, the values of the effective interlayer tunneling parameters should be lower in order to better describe real twisted bilayers [23]. The strong values of V that we are using are needed in order to observe a clear TRSB phase in our system [1,2]. However, the effective model used here allows us to probe the range of parameters needed for chiral superconductivity to be observable.

The interlayer bias term takes the form

$$H_\epsilon = -\epsilon \sum_{\mathbf{r},\sigma} (n_{\mathbf{r},1,\sigma} - n_{\mathbf{r},2,\sigma}). \qquad (5)$$

This contribution effectively shifts the chemical potential on each layer by $\pm\epsilon$. The density n_ℓ in each layer is then different from the total density n. The transformation $\epsilon \rightarrow -\epsilon$ effectively swaps both layers so we can concentrate on positive values of ϵ.

The two layers are assumed to have the same lattice constant. Different lattice constants would not lead to a commensurate unit cell with a reasonable number of orbitals with twist angle close to 45°.

Model (1) is applied to the bilayer with twist angle $\theta = 53.13°$. At this twist angle, the unit cell of the bilayer system is made of 10 sites, as illustrated in Fig. 1. That twist angle was chosen over 43.60° because of the relatively low computing resources needed.

The superconducting phase in this model is probed using the VCA [25,26] with an exact-diagonalization solver at zero temperature, like in Refs [1,2]. This variational method on the electron self-energy, based of Potthoff's self-energy functional approach, allows us to probe broken symmetries while preserving strong correlations. It has been used to study magnetic phases [26,27] and superconductivity [28,29] in
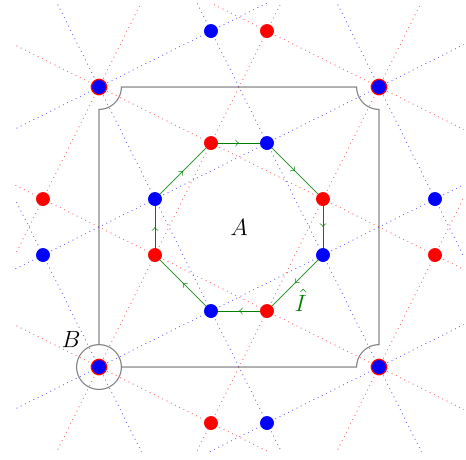

FIG. 1. Unit cell of the twisted bilayer cuprate system at $\theta = 53.13°$, containing 10 sites between the two layers. The top (bottom) layer correspond to the blue (red) lattice. The A clusters contain eight sites and the B cluster contains only two sites that are on top of each other. The green arrow show the direction of the current defined by Eq. (9).

various systems. For a detailed review of the method, see Refs. [1,30,31].

As shown in Ref. [1], we expect the superconducting order parameter of the bilayer system to belong to the irreducible representations B_1 or B_2 of the D_4 point group of the bilayer. We define the VCA Weiss field belonging to these two representations as

$$\hat{B}_1 = \hat{\Delta}^{(1)} + \hat{\Delta}^{(2)}, \quad \hat{B}_2 = \hat{\Delta}^{(1)} - \hat{\Delta}^{(2)}, \qquad (6)$$

where the d-wave pairing operator on layer l is defined as

$$\hat{\Delta}^{(\ell)} = \sum_{\mathbf{r} \in \ell} c_{\mathbf{r},\ell,\uparrow} c_{\mathbf{r}+\mathbf{x}^{(\ell)},\ell,\downarrow} - c_{\mathbf{r},\ell,\downarrow} c_{\mathbf{r}+\mathbf{x}^{(\ell)},\ell,\uparrow}$$
$$- c_{\mathbf{r},\ell,\uparrow} c_{\mathbf{r}+\mathbf{y}^{(\ell)},\ell,\downarrow} + c_{\mathbf{r},\ell,\downarrow} c_{\mathbf{r}+\mathbf{y}^{(\ell)},\ell,\uparrow}. \qquad (7)$$

For a more detailed description and justification of these definitions, see Refs. [1,2].

In the VCA procedure, we can use $\hat{B}_1$ or $\hat{B}_2$ to probe the superconducting phase. One of them should lead to a lower-energy state and be favored. It is also possible that the complex combination $\hat{B}_1 + i\hat{B}_2$ lowers the energy even more; this combination corresponds to the TRSB state. In such cases, we can express the relative phase ϕ between the order parameters $\langle \hat{\Delta}^{(1)} \rangle$ and $\langle \hat{\Delta}^{(2)} \rangle$ of the two planes as

$$\tan\frac{\phi}{2} = \frac{\text{Im}\psi_{B_2}}{\text{Re}\psi_{B_1}}, \qquad (8)$$

with ψ_{B_i} the order parameter $\psi_{B_i} = \frac{1}{L}\langle \hat{B}_i \rangle$, where L is the number of site and $i = 1, 2$. A value of $\phi = 0$ ($\phi = \pi$) corresponds to a pure B_1 (B_2) case. The interesting case is the one where $\phi \neq 0$ or π, where there is a coexistence of both states, indicating a TRSB.

We use the VCA procedure with Weiss fields from both representations (B_1 and B_2), with varying values of ϵ, to probe the effect of different layer-doping content on the TRSB phase.
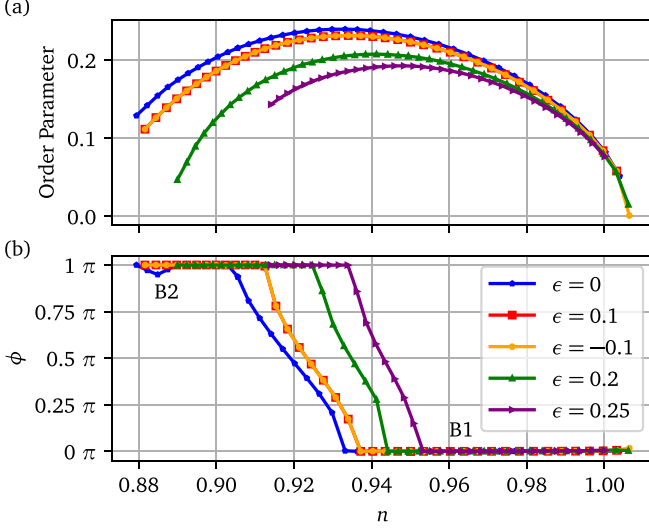
FIG. 2. Superconducting order parameter as a function of electron density n in the twisted cuprate bilayer at $\theta = 53.13°$ for different interlayer bias parameters ϵ. (a) Norm $\sqrt{|\psi_1|^2 + |\psi_2|^2}$ of the order parameter obtained from the VCA procedure with both representation as Weiss field for different values of ϵ. The order parameter drops when $|\epsilon|$ increases. (b) Relative phase ϕ between the two layers. We observe a shift in the range of the TRSB close to half filling ($n = 1$) when $|\epsilon|$ increases.

III. RESULT AND DISCUSSION

A. Interlayer bias

Figure 2 shows the superconducting order parameter and relative phase ϕ as a function of electron density in model (1) with $\theta = 53.13°$, for different values of ϵ. In Fig. 2(a), we observe that the difference in doping between the two layers causes a drop of the order parameter. Assuming a monotonous relation between the order parameter and the critical temperature T_c, we can infer that T_c should be maximal when $\epsilon = 0$ (when both layers are identical). As expected from the symmetry of the system, the effect depends on the absolute value $|\epsilon|$ only. This can also be seen in Fig. 2(b), where we show the relative phase ϕ. The TRSB phase corresponds to the region where $\phi \neq 0$ or π. We observe a shift in the TRSB region towards half filling with increasing $|\epsilon|$. While increasing $|\epsilon|$, the TRSB doping range also becomes narrower, making it more difficult to detect at high values of bias ϵ. If the doping discrepancy between the two layers is too large, the system may not show the TRSB behavior. This might explain the difficulty to observe a nonzero critical current in some 45° c-axis Josephson junctions [14–17].

For all values of ϵ considered, the TRSB occurs in the overdoped region, i.e., beyond optimal doping according to Fig. 2, in at least one of the layers. There are theoretical signs that the superconducting states in the under- and overdoped regions are qualitatively different, even though they share the same symmetry [32]. Correlation effects being lower in the overdoped region, the superconducting state is closer to the BCS state than in the underdoped region. This seem to impact the TRSB phase.
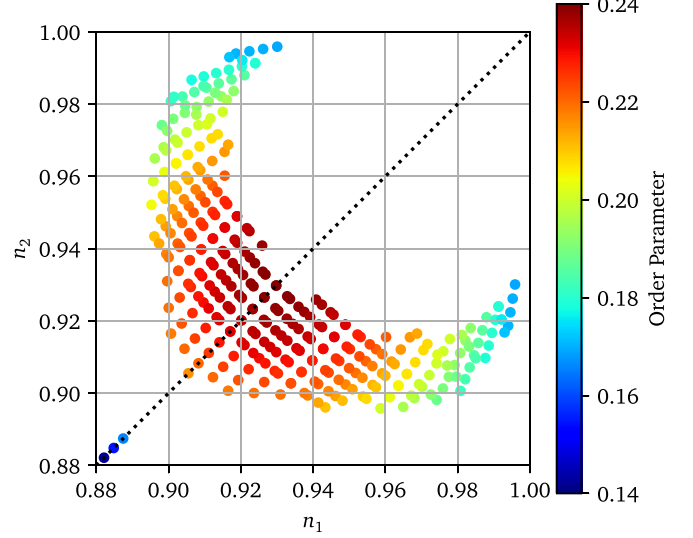

FIG. 3. Phase diagram of the TRSB phase for different sets of layer doping (n_1, n_2). The points indicate that a nontrivial relative phase was found with this combination of layer dopings. The color map represents the order parameter. The order parameter is maximum when the bias $|\epsilon|$ vanishes (dotted line).

In Fig. 3, we show a map of the TRSB phase as a function of doping $n_{1,2}$ on each layer. The diagram has a crescent form and is symmetric around the zero bias ($\epsilon = 0$), corresponding to $n = n_1 = n_2$. The order parameter drops when deviating from $\epsilon = 0$, as seen in Fig. 2.

The distribution of the TRSB phase is not uniform. In fact, some combinations offer a bigger tolerance to doping differences. Indeed, when one of the layers is in the overdoped region $n_\ell \in [0.90, 0.92]$, TRSB occurs in a larger interval of doping for the second layer. On the other hand, near the tips of the crescent, the system has a small tolerance to doping difference and a TRSB phase will be hard to observe.

The three points close to $n = 0.88$ on the dotted line correspond to the small bump seen in Fig. 2 for $\epsilon = 0$. We believe that those results are an artifact of the method and do not hold physical meaning since no other values of ϵ exhibit this behavior.

B. Interlayer current

It is possible to define an interlayer current operator $\hat{I}$ between the sites of the different layers on cluster A as

$$\hat{I} = i \sum_{\{\mathbf{r},\mathbf{r}'\}_I} (c^\dagger_{\mathbf{r},1,\sigma} c_{\mathbf{r}',2,\sigma} - c^\dagger_{\mathbf{r}',2,\sigma} c_{\mathbf{r},1,\sigma}), \qquad (9)$$

where $\{\mathbf{r}, \mathbf{r}'\}_I$ is the set of pairs of sites defining the green path in Fig. 1. This operator can be used to extract information related to a Josephson current, with the order parameter given by $I = \frac{1}{L}\langle\hat{I}\rangle$. Experimentally, a nonzero Josephson current appears when the relative phase between both layers is nontrivial. The maximal current corresponds to a relative phase of $\phi = \frac{\pi}{2}$. This behavior is observed within our data while using Eq. (9) as the definition of our Josephson current.

Figure 4 shows the phase diagram for different sets of layer doping (n_1, n_2). The points indicate that a current $|I| > 10^{-4}$
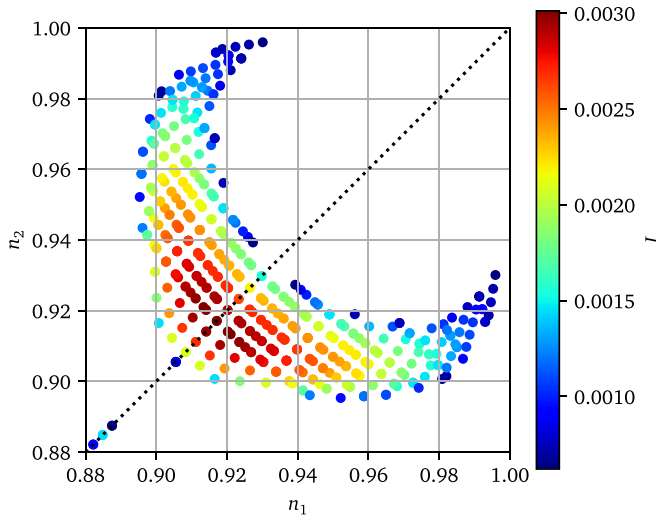
FIG. 4. Map of the spontaneous current I along the loop defined in Fig. 1 for different sets of layer doping (n_1, n_2). A dot indicates a nonzero spontaneous current ($|I| > 10^{-4}$) and the color map represents the value of the current. The dotted line corresponds to $\epsilon = 0$.

was found, whose intensity is mapped in color. This criterion makes sure that the current is significantly larger than the numerical precision (10^{-7}). The current is maximum when ϕ is close to $\frac{\pi}{2}$ and when the two layers have similar doping levels. The crescent has the same shape as in Fig. 3, except that the current falls to zero outside of the crescent, whereas the superconducting order parameter does not. The current is indeed an order parameter for TRSB. The choice of current loop in Fig. 1 is not the only one possible. Other closed paths between the two layers would yield similar results, except for the overall current amplitude. Without external bias, we expect the net current between the two layers to vanish.

C. Topology

We investigated the topological nature of the TRSB phase by computing the Chern number using the Green function obtained from the VCA [33,34]. Unfortunately, we found that the topology is always trivial in the region of interest: The Chern number vanishes. The Brillouin zone has regions of opposite Berry curvature that compensate exactly, despite the system being clearly gapped everywhere. A typical plot of the Berry curvature is shown on the left panel of Fig. 5, where regions of opposite signs are evident; so is the full superconducting gap, as shown on the right panel. The trivial topology is likely due to the strong interaction regime that applies here; topologically nontrivial to trivial transitions as U increases have been theoretically observed in other systems [35].

D. Effect of t' and U

The value of the next-nearest-neighbor hopping (t') was chosen to best describe Bi2212. It is possible to change this value to probe the effect of considering different compounds. We looked at two other values of t' (-0.2 and -0.45) while keeping every other parameter the same ($t = 1$, $U = 8$, and
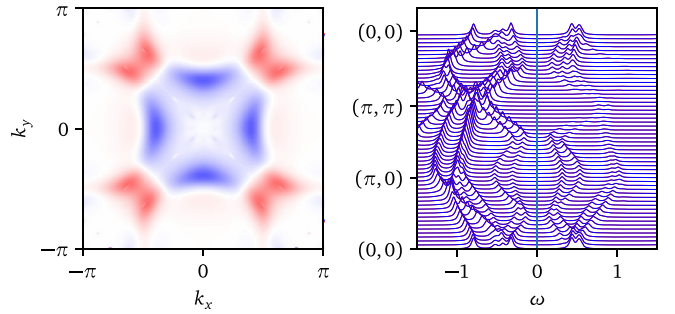

FIG. 5. Left panel: Color plot of the Berry curvature in the Brillouin zone (blue is negative, red is positive). The integrated Berry curvature (the Chern number) vanishes. Right panel: Corresponding spectral function along high-symmetry axes. The superconducting gap is very clear. The parameters are $U = 8$, $V = 0.4$, $e = 0$, and $\mu = 1.34$ ($n = 0.923$).

$V = 0.4$). We also looked at the effect of varying U ($U = 7$) while keeping $t' = -0.3$.

Figure 6 show the relative phase ϕ obtained by VCA for two other values of t' and for $U = 7$. The doping range where the TRSB phase is observed is shifted when t' is changed from -0.3. For $t' = -0.2$, the region is shifted toward higher doping, while for $t' = -0.45$, it is shifted toward half filling.
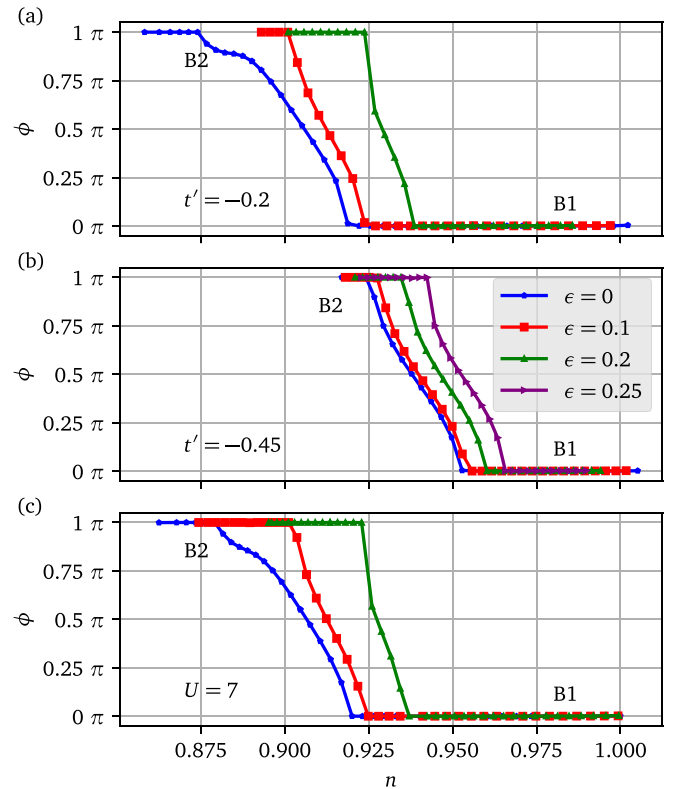

FIG. 6. (a) Relative phase ϕ between the two layers for $t' = -0.2$. The TRSB region is shifted to higher doping compared to $t' = -0.3$ (Fig. 2). (b) Relative phase ϕ between the two layers for $t' = -0.45$. In this case, the TRSB region is shifted to lower doping compared to to $t' = -0.3$. (c) Relative phase ϕ between the two layers for $U = 7$. The TRSB region is shifted toward higher doping compared to $U = 8$.
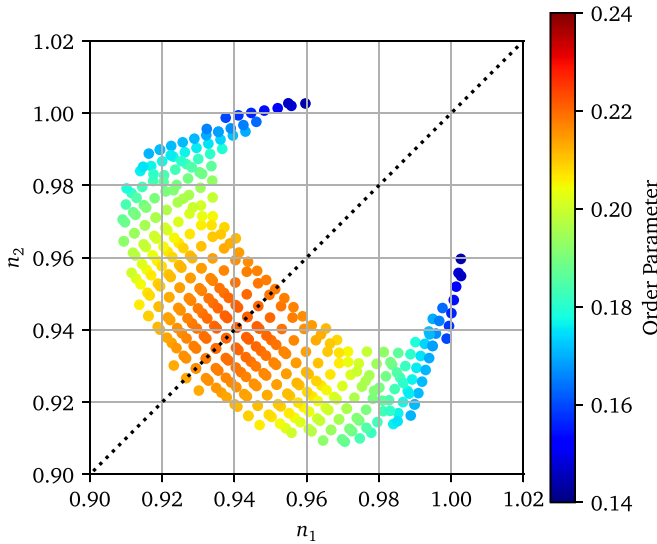
FIG. 7. Phase diagram of the TRSB phase for different sets of layer density (n_1, n_2) for $t' = -0.45$. The features observed here are similar to what is observed for $t' = -0.3$ (Fig. 3).

At $U = 7$, the TRSB phase is shifted toward higher doping compared to $U = 8$. This was also observed in Ref. [2]. This shows that the TRSB phase is robust against changes in the dispersion or interaction strength.

Figure 7 shows the phase diagram of the TRSB phase for combinations of layer density (n_1, n_2) for $t' = -0.45$. The shape of the diagram is similar to that for $t' = -0.3$, but shifted closer to half filling. Some data points show a density $n_\ell > 1$, which can be attributed to the error on the electron density typical of VCA when the chemical potential within the cluster is not treated as an additional variational parameter.

From the results presented here for model (1), it is possible to explain the sensibility of the cuprate Josephson junction

to impurities and doping. At the same time, if one layer is in the high-tolerance region, the TRSB phase could be easier to obtain. We note that our model is an oversimplification of the cuprate bilayer since it is based on the one-band Hubbard model and ignores the fact that each layer of the twisted system is, in fact, itself a bilayer. Still, we hope that the effects of doping asymmetry presented here are robust.

IV. CONCLUSION

We used a one-band Hubbard model describing twisted bilayer cuprates at $\theta = 53.13°$ with an interlayer bias ϵ, simulating a doping asymmetry between layers. Using the variational cluster approach, we probed the superconducting phase and found that $|\epsilon|$ affects the doping range and order parameter of the time-reversal symmetry-breaking state. We use the spontaneous current along a small loop as a TRSB order parameter. Increasing the interlayer bias pushes the TRSB region towards half filling, while making it narrower. The SC order parameter also decreases when the interlayer bias increases. Overall, the TRS region has a crescent shape in the n_1-n_2 plane ($n_{1,2}$ being the electron densities on layers 1 and 2). One of the layers has to be in the overdoped region for the bilayer to break time reversal. But once a layer is overdoped, there is some tolerance to a doping difference with the other layer.

[1] X. Lu and D. Sénéchal, Phys. Rev. B **105**, 245127 (2022).

[2] M. Bélanger and D. Sénéchal, Phys. Rev. B **109**, 045111 (2024).

[3] O. Can, T. Tummuru, R. P. Day, I. Elfimov, A. Damascelli, and M. Franz, Nat. Phys. **17**, 519 (2021).

[4] P. A. Volkov, J. H. Wilson, K. P. Lucht, and J. H. Pixley, Phys. Rev. B **107**, 174506 (2023).

[5] X.-Y. Song, Y.-H. Zhang, and A. Vishwanath, Phys. Rev. B **105**, L201102 (2022).

[6] M. Fidrysiak, B. Rzeszotarski, and J. Spałek, Phys. Rev. B **108**, 224509 (2023).

[7] G. Margalit, B. Yan, M. Franz, and Y. Oreg, Phys. Rev. B **106**, 205424 (2022).

[8] A. Mercado, S. Sahoo, and M. Franz, Phys. Rev. Lett. **128**, 137002 (2022).

[9] Y.-X. Li and C.-C. Liu, Phys. Rev. B **107**, 235125 (2023).

[10] V. Brosco, G. Serpico, V. Vinokur, N. Poccia, and U. Vool, Phys. Rev. Lett. **132**, 017003 (2024).

[11] T. Tummuru, E. Lantagne-Hurtubise, and M. Franz, Phys. Rev. B **106**, 014520 (2022).

[12] Y. Yu, L. Ma, P. Cai, R. Zhong, C. Ye, J. Shen, G. D. Gu, X. H. Chen, and Y. Zhang, Nature (London) **575**, 156 (2019).

[13] S. Y. Frank Zhao, N. Poccia, M. G. Panetta, C. Yu, J. W. Johnson, H. Yoo, R. Zhong, G. D. Gu, K. Watanabe, T. Taniguchi, S. V. Postolova, V. M. Vinokur, and P. Kim, Phys. Rev. Lett. **122**, 247001 (2019).

[14] J. Lee, W. Lee, G.-Y. Kim, Y.-B. Choi, J. Park, S. Jang, G. Gu, S.-Y. Choi, G. Y. Cho, G.-H. Lee, and H.-J. Lee, Nano Lett. **21**, 10469 (2021).

[15] M. Martini, Y. Lee, T. Confalone, S. Shokri, C. N. Saggau, D. Wolf, G. Gu, K. Watanabe, T. Taniguchi, D. Montemurro, V. M. Vinokur, K. Nielsch, and N. Poccia, Mater. Today **67**, 106 (2023).

[16] Y. Lee, M. Martini, T. Confalone, S. Shokri, C. N. Saggau, D. Wolf, G. Gu, K. Watanabe, T. Taniguchi, D. Montemurro, V. M. Vinokur, K. Nielsch, and N. Poccia, Adv. Mater. **35**, 2209135 (2023).

[17] S. Y. Frank Zhao, N. Poccia, X. Cui, P. A. Volkov, H. Yoo, R. Engelke, Y. Ronen, R. Zhong, G. Gu, S. Plugge, T. Tummuru, M. Franz, J. H. Pixley, and P. Kim, Science **382**, 1422 (2023).

[18] P. A. Volkov, S. Y. F. Zhao, N. Poccia, X. Cui, P. Kim, and J. H. Pixley, arXiv:2108.13456.

[19] T. Tummuru, S. Plugge, and M. Franz, Phys. Rev. B **105**, 064501 (2022).

[20] A. C. Yuan, Y. Vituri, E. Berg, B. Spivak, and S. A. Kivelson, Phys. Rev. B **108**, L100505 (2023).

[21] D. A. Ruiz-Tijerina and V. I. Fal'ko, Phys. Rev. B **99**, 125424 (2019).

[22] Y. Tang, L. Li, T. Li, Y. Xu, S. Liu, K. Barmak, K. Watanabe, T. Taniguchi, A. H. MacDonald, J. Shan, and K. F. Mak, Nature (London) **579**, 353 (2020).

[23] R. S. Markiewicz, S. Sahrakorpi, M. Lindroos, H. Lin, and A. Bansil, Phys. Rev. B **72**, 054519 (2005).

[24] D. Sénéchal, A. G. R. Day, V. Bouliane, and A.-M. S. Tremblay, Phys. Rev. B **87**, 075123 (2013).

[25] M. Potthoff, M. Aichhorn, and C. Dahnken, Phys. Rev. Lett. **91**, 206402 (2003).

[26] C. Dahnken, M. Aichhorn, W. Hanke, E. Arrigoni, and M. Potthoff, Phys. Rev. B **70**, 245110 (2004).

[27] P. Sahebsara and D. Sénéchal, Phys. Rev. Lett. **100**, 136402 (2008).

[28] J. P. L. Faye and D. Sénéchal, Phys. Rev. B **95**, 115127 (2017).

[29] M. Bélanger, J. Fournier, and D. Sénéchal, Phys. Rev. B **106**, 235135 (2022).

[30] M. Potthoff, in *Strongly Correlated Systems: Theoretical Methods*, edited by A. Avella and F. Mancini (Springer, Berlin, 2012), Vol. 171, pp. 303–339.

[31] M. Potthoff, in *DMFT at 25 Infinite Dimensions Lecture Notes of the Autumn School on Correlated Electrons 2014*, edited by E. Pavarini, E. Koch, D. Vollhardt, and A. I. Lichtenstein, Jülich Research Center, Series Modeling and Simulation Vol. 4 (Forschungszentrum Jülich Publishing, Jülich, 2014).

[32] S. S. Dash and D. Sénéchal, Phys. Rev. B **100**, 214509 (2019).

[33] Z. Wang and S.-C. Zhang, Phys. Rev. X **2**, 031008 (2012).

[34] Z. Wang and S.-C. Zhang, Phys. Rev. B **86**, 165116 (2012).

[35] J. Wu, Jean Paul Latyr Faye, D. Sénéchal, and J. Maciejko, Phys. Rev. B **93**, 075131 (2016).